Facilitated Transport of Copper with Hydroxyapatite Nanoparticles in Saturated Sand

Dengjun Wang
Key Lab. of Soil Environment and Pollution Remediation
Institute of Soil Science
Chinese Academy of Sciences
No. 71 East Beijing Rd.
Nanjing 210008, China
and
Graduate School of the Chinese Academy of Sciences
Beijing 100049, China

Scott A. Bradford
USDA-ARS
U.S. Salinity Lab.
450 W. Big Springs Rd.
Riverside, CA 92507

Marcos Paradelo
Soil Science Group
Dep. of Plant Biology and Soil Science
Faculty of Sciences
Univ. of Vigo
Ourense E-32004, Spain

Willie J.G.M. Peijnenburg
Lab. of Ecological Risk Assessment
National Institute of Public Health and the Environment
P.O. Box 1
3720 BA Bilthoven, the Netherlands
and
Institute of Environmental Sciences
Leiden Univ.
P.O. Box 9518
2300 RA Leiden, the Netherlands

Dongmei Zhou*
Key Lab. of Soil Environment and Pollution Remediation
Institute of Soil Science
Chinese Academy of Sciences
No. 71 East Beijing Rd.
Nanjing 210008, China

Saturated packed column experiments were conducted to investigate the facilitated transport of Cu with hydroxyapatite nanoparticles (nHAP) at different pore water velocities (0.22–2.2 cm min^{-1}), solution pH (6.2–9.0), and fraction of Fe oxide coating on grain surfaces (λ, 0–0.36). The facilitated transport of Cu by nHAP (nHAP-F Cu) was found to increase with decreasing nHAP retention and decreasing transport of dissolved Cu. In particular, nHAP-F Cu transport increased with pH (8.0, 8.5, and 9.0) and especially λ (0.07–0.36) but was less significant than dissolved Cu transport at lower pH (6.2 and 7.0). The transport of dissolved Cu decreased with pH and λ because of increased Cu sorption or precipitation. The nHAP retention decreased with velocity, pH, and decreasing λ. Scanning electron microscope images revealed that nHAP retention at pH 7.0 was controlled by surface roughness and nHAP aggregation, whereas measured zeta potentials indicate that attachment of the nHAP occurred on the Fe oxide coated grains. The retention profiles of nHAP exhibited a hyperexponential shape, with greater retention in the section adjacent to the column inlet and rapidly decreasing retention with depth for all of the considered pH and λ conditions, but tended to become more exponential in shape at a higher velocity. These observations suggest that hyperexponential profiles are a general phenomenon of unfavorable attachment conditions that is sensitive to the hydrodynamics at the column inlet.

Abbreviations: BTC, breakthrough curve; CFT, colloid filtration theory; EDX, energy dispersive x-ray; IS, ionic strength; nHAP, hydroxyapatite nanoparticles; nHAP-F Cu, hydroxyapatite nanoparticle facilitated copper; PV, pore volume; RP, retention profile; SEM, scanning electron microscopy.

Hydroxyapatite nanoparticles [$Ca(PO_4)_6(OH)_2$] have been widely used to remediate soils and wastewater contaminated by metals such as Cu, Zn, Pb, Cd, and Co (Ma et al., 1994; Smičiklas et al., 2006; Wang et al., 2009). The fixation of metal ions on nHAP may take place through ion exchange, surface complexation, dissolution of nHAP to form new metal phosphates, and substitution of the Ca^{2+} ions in nHAP by other metal ions during recrystallization (Ma et al., 1994; Smičiklas et al., 2006). The small size and high surface area of nHAP make these particles especially reactive sorbents. Little attention has been paid, however, to potential environmental risks of nHAP during soil remediation. For example, nHAP significantly changes the distribution of metal contaminants, such as Cu, among the mobile and immobile phases (Wang et al., 2011a). The transport of many chemicals can be greatly enhanced when they are associated with mobile colloids (McCarthy and Zachara, 1989; Grolimund et al., 1996; Roy and Dzombak, 1997; Kretzschmar et al., 1999; de Jonge et al., 2004; Šimůnek et al., 2006; Bradford and Kim, 2010; Wang et al., 2011b) such as nHAP.

Soil Sci. Soc. Am. J. 76:375–388
Posted online 20 Dec. 2011
doi:10.2136/sssaj 2011.0203
Received 3 June 2011
*Corresponding author (dmzhou@issas.ac.cn)

Little information is currently available about the facilitated transport potential of Cu by nHAP in subsurface environments (Wang et al., 2011b), especially with regard to solution velocity, pH, and soil surface charge heterogeneities. Variations in solution velocity, pH, and surface charge heterogeneities are common in natural and engineered aquatic environments as a result of variations in soil texture and structure, recharge rates, aqueous and solid-phase geochemistry, and biological factors (McCarthy and Zachara, 1989; Johnson et al., 1996; Kretzschmar et al., 1999; Elimelech et al., 2000; Abudalo et al., 2010). Colloid filtration theory (CFT) (Yao et al., 1971) predicts that the rate of colloid attachment and mass transfer to solid surfaces will be a function of the solution velocity. The most common source of surface charge heterogeneity in natural aquatic environments is Fe and Al oxyhydroxides, which are amphoteric minerals with relatively high points of zero charge (pH_{PZC}) (Parks, 1965). Typical pH values in aquatic environments are below their pH_{PZC}; therefore, these minerals adsorb protons and acquire a net positive surface charge (Johnson et al., 1996; Abudalo et al., 2010). Most engineered nanoparticles and silica minerals exhibit a net negative surface charge at ambient pH values (Petosa et al., 2010). Hence, electrostatic conditions for nHAP attachment are expected to be "unfavorable" for negatively charged silica surfaces and "favorable" for positively charged Fe and Al oxyhydroxides. Changes in the solution pH, however, can alter the surface charge of mineral surfaces and nHAP, thereby influencing the nHAP attachment behavior.

An understanding of nHAP retention mechanisms is needed to select or develop mathematical models to accurately describe and predict the transport of nHAP and the facilitated transport of Cu. In particular, models need to accurately capture the nHAP breakthrough curves (BTCs) and retention profiles (RPs) with distance. The CFT assumes an exponential decrease in colloid retention with transport distance (Yao et al., 1971). In contrast, experimental RPs are frequently not exponential with distance (Tufenkji et al., 2003). The shape of RPs has been reported to be sensitive to heterogeneity in the colloid population and in the collector grain surface (Baygents et al., 1998; Simoni et al., 1998; Silliman et al., 2001; Li et al., 2004; Tufenkji and Elimelech, 2005) and the system hydrodynamics (Torkzaban et al., 2007, 2008; Bradford et al., 2011) under unfavorable attachment conditions. Various hypotheses have been proposed in the literature to account for the observed deviations from CFT predictions (Baygents et al., 1998; Simoni et al., 1998; Silliman et al., 2001; Bradford et al., 2003, 2009b; Tufenkji et al., 2003; Li et al., 2004; Tufenkji and Elimelech, 2005; Chatterjee and Gupta, 2009).

The main objective of this study was to systemically investigate the effects of solution velocity, pH, and Fe oxide grain coatings on the transport of Cu in association with nHAP in water-saturated packed quartz columns. A secondary objective was to investigate mechanisms of nHAP retention and to test hypotheses with regard to the causes of hyperexponential (decreasing rate of retention with distance) RPs.

MATERIALS AND METHODS

Porous Media

For the velocity and pH experiments, quartz sand was obtained from a commercial supplier (Sinopharm Chemical Reagent Co. Ltd., 26–30 mesh, 0.55–0.65 mm). The median grain size was 0.6 mm, and the coefficient of uniformity was 1.3 ($U_i = d_{60}/d_{10}$, where x % of the mass is finer than d_x). Before use, the sand was cleaned thoroughly to remove any metal oxide and adsorbed clay on the grain surface using a procedure described elsewhere (Zhou et al., 2011). Briefly, the sand was ultrasonicated in 0.01 mol L^{-1} NaOH solution for 30 min, rinsed with deionized water, and then ultrasonicated again for an additional 30 min in 0.01 mol L^{-1} HCl solution before a final thorough rinsing with deionized water. The sand was then dried in an oven at 100°C.

Surface charge heterogeneity is usually introduced into a model porous medium by coating a fraction of the grains with Fe oxyhydroxide (Johnson et al., 1996; Abudalo et al., 2010). Some of the quartz sand was therefore coated with Fe oxide following a procedure similar to that used by Stahl and James (1991). Briefly, Fe oxide was precipitated onto 500 g of quartz sand by adding 87.5 mL of 0.17 mol L^{-1} $Fe(NO_3)_3$ and 90.0 mL of 0.52 mol L^{-1} NaOH in an evaporating dish. The mixture was placed in a drying oven at 105°C for 72 h. The mixture was stirred periodically to prevent crusting of the salts on the surface. After coating the quartz sand with Fe oxide, the coated sand was washed in 1.0 mmol L^{-1} HCl and then 1.0 mmol L^{-1} NaOH to remove weakly absorbed Fe on the sand surface. Examination of individual coated grains by scanning electron microscopy–energy dispersive x-ray (SEM-EDX) analysis (SSX-550, Shimadzu Corp., Tokyo) showed that 75 ± 3% of the grain surfaces were coated by Fe oxide (see Fig. 1). The amount of Fe on the coated and uncoated sand was determined by a partial acid digestion (16 mol L^{-1} HNO_3 and 30% H_2O_2). The Fe concentration was measured in the digestion solution using an atomic absorption spectrophotometer (Z-2000, Hitachi High-Technologies Corp., Tokyo). Chemically heterogeneous porous media were prepared by mixing portions of the coated and uncoated sand to achieve Fe oxide surface coverage ranging from $\lambda = 0$ to 0.36 (see Table 1) for facilitated transport experiments (Elimelech et al., 2000). The coating of 75% of the grain surface is accounted for in λ.

Copper-Bearing Hydroxyapatite Nanoparticles Suspension Preparation

Hydroxyapatite nanoparticles (+99%, Nanjing Aipurui Nanomaterial Co., Nanjing, China) with a nominal size of 20-nm diameter and 100-nm length were used in all experiments. The physicochemical properties of the nHAP were determined in our previous work (Wang et al., 2011a). Briefly, the Ca/P molar ratio was 1.65 and the specific surface area of the nHAP was 154 $m^2\ g^{-1}$.

Stable, Cu-bearing nHAP suspensions were prepared by adding 0.10 g of nHAP powder to 500 mL of solution containing 0.10 mmol L^{-1} $Cu(NO_3)_2$ (analytical grade) and 1.0 mmol L^{-1} NaCl. The pH of the Cu-bearing

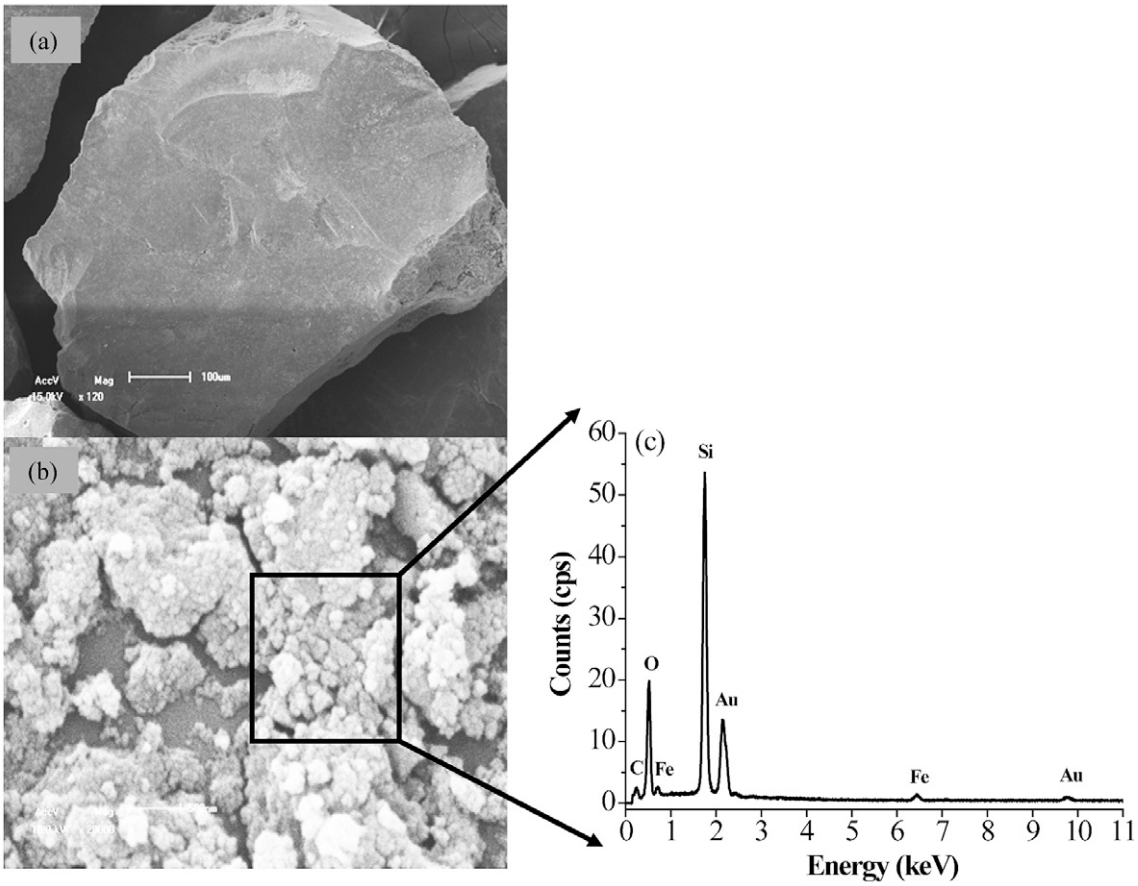

Fig. 1. Scanning electron micrographs of (a) uncoated quartz sand, (b) Fe oxide coated quartz sand used in the column experiments, and (c) the corresponding energy dispersive x-ray spectrum of the Fe oxide grain coating on the quartz sand in the box.

nHAP suspensions was adjusted while mixing by incrementally adding 1.0 mmol L^{-1} NaOH to achieve pH values of 6.2, 7.0, 8.0, 8.5, and 9.0 (Table 1). Transport experiments with nHAP that examined the influence of pH were conducted at these pH values, whereas those investigating the influence of velocity and Fe oxide sand coatings were conducted only at pH 6.2. The concentrations of nHAP and Cu in the resulting stable suspensions were 200 mg L^{-1} and 0.10 mmol L^{-1}, respectively. Before use, the suspensions were homogenized by stirring on a magnetic plate for 1 min and sonicated in a water bath (100 W, 45 kHz, KQ-

Table 1. Electrokinetic potentials of sand grains (ζ_g) and Cu-bearing hydroxyapatite nanoparticles (ζ_{nHAP}), and Derjaguin–Landau–Verwer–Overbeek (DLVO) parameters for the nHAP–sand interaction under different pore water velocity (v), pH, and Fe oxide grain coating fraction (λ) conditions.

v	pH	λ	Ionic strength	ζ_g	ζ_{nHAP}	A†	Φ_{max} KT‡	Φ_{min2} KT‡	h§
cm min^{-1}			mmol L^{-1}	mV		J			nm
0.22	6.2	0	0.1	−62.4 ± 1.6	−39.5 ± 1.9	5.54×10^{-21}	142	−0.774	54
0.44	6.2	0	0.1	−62.4 ± 1.6	−39.5 ± 1.9	5.54×10^{-21}	142	−0.774	54
2.2	6.2	0	0.1	−62.4 ± 1.6	−39.5 ± 1.9	5.54×10^{-21}	142	−0.774	54
0.44	7.0	0	0.1	−71.9 ± 2.1	−42.7 ± 2.6	5.54×10^{-21}	172	−0.718	61
0.44	8.0	0	0.1	−76.0 ± 2.3	−47.0 ± 1.9	5.54×10^{-21}	207	−0.716	60
0.44	8.5	0	0.1	−78.3 ± 1.8	−51.2 ± 1.7	5.54×10^{-21}	240	−0.713	60
0.44	9.0	0	0.1	−81.2 ± 2.7	−54.3 ± 1.7	5.54×10^{-21}	268	−0.710	59
0.44	6.2	0.07	0.1	−56.3 ± 1.3	−39.5 ± 1.9	9.98×10^{-21}	131	−1.30	57
0.44	6.2	0.14	0.1	−50.2 ± 0.9	−39.5 ± 1.9	9.98×10^{-21}	124	−1.15	66
0.44	6.2	0.22	0.1	−43.2 ± 1.4	−39.5 ± 1.9	9.98×10^{-21}	114	−1.21	61
0.44	6.2	0.29	0.1	−37.0 ± 0.8	−39.5 ± 1.9	9.98×10^{-21}	96	−1.23	60
0.44	6.2	0.36	0.1	−30.1 ± 0.6	−39.5 ± 1.9	9.98×10^{-21}	68	−1.21	60

† Hamaker constant.

‡ Φ_{max} and Φ_{min2}, energy barrier to the primary minimum and the depth of the secondary minimum as calculated by DLVO theory, K is the Boltzmann constant, and T is the absolute temperature.

§ Separation distance for the secondary minimum.

300VDE, Kunshan Sonicator Co., Shanghai, China) at room temperature for 30 min.

Adsorption Isotherms of Copper(II) on Hydroxyapatite Nanoparticles

The adsorption isotherm of Cu(II) on the nHAP at different ionic strengths and pH 6.2 was performed previously (Wang et al., 2011a). In this work, the adsorbed quantity of Cu(II) on nHAP at different suspension pHs was performed by adding 0.010 g of nHAP powder to 50 mL of 0.1 mmol L^{-1} $Cu(NO_3)_2$ and 0.1 mmol L^{-1} NaCl in a centrifuge tube. The pH of the Cu-bearing nHAP suspensions was adjusted while mixing by incrementally adding 1.0 mmol L^{-1} HCl or NaOH to achieve pH values of 5.0, 6.2, 7.0, 8.0, 8.5, and 9.0. All the experiments were conducted in triplicate.

The centrifuge tubes were continuously shaken for 12 h at 25°C. Aliquots (5 mL) of all suspensions were centrifuged at 170,000 × *g* for 1 h (Optima L-80XP Ultracentrifuge, Beckman Coulter, Brea, CA) and then filtered through a 0.22-μm membrane filter to determine the dissolved Cu. The concentration of Cu associated with the nHAP (nHAP-F Cu) was calculated as the difference between the total and dissolved Cu. The Cu concentration was determined using an atomic absorption spectrophotometer.

Columns

The facilitated transport experiments were conducted in glass chromatography columns (2.6-cm diameter and 20-cm length, Shanghai Huxi Glassware Co., Shanghai, China) with polytetrafluoroethene end caps and stainless steel mesh (80-μm openings) on both ends of the column. To pack the columns, sand grains were added to about 1 to 2 cm of standing water in the column in 1-cm lifts. After each lift, the columns were tapped to eliminate air bubbles. In the Fe oxide coating experiments, the coated and uncoated sand grains were thoroughly mixed to ensure an even distribution in the column. The porosity was determined by the difference in mass between a saturated and a dry-packed column and confirmed by analysis of a tracer (Br^-) BTC. The porosity of the packed columns varied between 0.40 and 0.42. The longitudinal dispersivity of the packed column was estimated from transport tests using Br^- as a tracer and ranged from 0.023 to 0.066 cm^2 min^{-1}.

Experimental Design

The packed columns were initially equilibrated by flushing several pore volumes (PVs) of ultrapure water and at least 5 PVs of nHAP-free background electrolyte solution (ionic strength [IS] = 0.1 mmol L^{-1}, see Table 1) to establish steady-state flow and to standardize the chemical conditions. Experiments were conducted in the following steps: (i) Phase 1, the Cu-bearing nHAP suspensions (Table 1) were gently stirred while being applied at the bottom end of the column via a peristaltic pump (YZΠ-15, Baoding Longer Precision Pump Co. Ltd., Hebei, China) at a constant fluid pore water velocity for about 3.75 PVs; and (ii) Phase 2, several PVs of nHAP-free background electrolyte solution with the same pH and IS were pumped into the column to ensure that almost no nHAP particles were detected in the effluent. For the velocity experiments, three different fluid pore water velocities (0.22, 0.44, and 2.2 cm min^{-1}) were considered to assess the influence of hydrodynamics on the facilitated transport of Cu by nHAP. The pH and Fe oxide coating experiments were conducted at a pore water velocity of 0.44 cm min^{-1}. Column outflow was collected into 15-mL glass tubes at regular time intervals using a fraction collector (BS-100A, Huxi Analytical Instrument Factory Co. Ltd., Shanghai, China). All facilitated transport tests were conducted in duplicate.

Following the completion of each transport test, the spatial distribution of nHAP retained in the column was determined. The end fitting was removed, and the quartz sands were carefully excavated in 2-cm increments and transferred into 10, 50-mL vials. For the experiments conducted at different velocities and pH values, excess ultrapure water was added to fill the vials. After 1 h, the vials containing the sand–nHAP solution mixture were gently shaken to obtain a homogeneous concentration of nHAP in the supernatant. The concentrations of nHAP in the excess aqueous solution were determined with a UV/Vis spectrophotometer (721-100, Jinghua Science and Technology Instrument Co. Ltd., Shanghai, China) at a wavelength of 300 nm (Chu et al., 2011; Wang et al., 2011a,b). A calibration curve was constructed by diluting the 200 mg L^{-1} nHAP suspension. The spectrometer response was linear with nHAP concentration in the range of 0 to 200 mg L^{-1}, with a coefficient of determination of $R^2 = 0.999$. The lower detection limit was 1.0 mg L^{-1}. The calibration curve was verified to be independent of the solution chemistry for our experimental conditions. For the Fe oxide coated sand experiments, 1.0 mmol L^{-1} HCl was added to the vials to dissolve the nHAP retained on the surface of the Fe oxide coating. The concentration of phosphate in the aqueous solution was then measured to calculate the concentration of nHAP. The sand samples were then oven dried at 20°C overnight to obtain the dry weight of the solid. A mass balance was calculated for nHAP in the effluent and retained in the sands after normalizing by the total amount of nHAP injected into the column.

After completion of the facilitated transport experiment with a suspension pH of 7.0 at a pore water velocity of 0.44 cm min^{-1}, some of the sand grains that were excavated from the inlet of the packed column were examined using SEM-EDX analysis to determine the mechanisms of nHAP retention in the column experiments.

Electrokinetic Properties of Hydroxyapatite Nanoparticles and Sand Grains

The electrokinetic potential (ζ potential) of Cu-bearing nHAP was measured following the procedure described elsewhere (Wang et al., 2011a,b). Briefly, triplicate Cu-bearing nHAP suspensions at fixed pH (Table 1) and IS were used for the microelectrophoresis instrument (JS94G, Shanghai Zhongcheng Digital Technology Co. Ltd., Shanghai, China) at 20°C. Streaming potentials of the Fe oxide coated sand grains were measured by using a streaming potential analyzer (BI-EKA,

Brookhaven Instruments Corp., Holtsville, NY). Detailed experimental procedures are given elsewhere (Elimelech et al., 2000; Abudalo et al., 2010). Streaming potentials were converted to ζ potentials using the Helmholtz–Smoluchowski equation (Johnson, 1999). This ζ potential information was used in conjunction with Derjaguin–Landau–Verwey–Overbeek (DLVO) theory (Derjaguin and Landau, 1941; Verwey and Overbeek, 1948) to calculate the average interaction energy of nHAP with the various porous media.

Concentrations of Hydroxyapatite Nanoparticles and Copper in the Effluent

The concentrations of nHAP in the outflow were determined using the 721-100 UV/Vis spectrophotometer at 300 nm, as described above.

Five milliliters of 16 mol L^{-1} HNO_3 was added to aliquots (5 mL) of all effluents to determine the total Cu concentration. The concentrations of dissolved Cu and nHAP-F Cu in the effluents were determined by the procedure described above.

The Br^- tracer, which was used to determine the hydrodynamic performance of the column, was analyzed using an ion-selective electrode for Br^- (PBr-1, Kangyi Instrument Co. Ltd., Shanghai, China). Based on the Br^- tracer concentration data, the fluid pore water velocity (v [L T^{-1}]) and the dispersion coefficient (D [L^2 T^{-1}]) were determined by fitting to the analytical solution of the standard convection–dispersion equation for a conservative solute (Toride et al., 1999).

Data Analysis

The fraction of mass recovery of the injected nHAP in the column outflow (M_{eff}) during Phases 1 and 2 was calculated by the zero moment of the nHAP BTC and normalizing it to the total amount injected (Walshe et al., 2010):

$$M_{\text{eff}}(\%)=\frac{\int_0^{\infty} Q(t)C(t)\,\mathrm{d}t}{\int_0^{T_0} Q(t)C_0(t)\,\mathrm{d}t} \qquad [1]$$

where Q is the flow rate [L^3 T^{-1}], C_0 and C are the concentration (nHAP or solute) in the injection solution and column outflow, respectively [M L^{-3} or no. L^{-3}], t is the time [T], and T_0 is the duration of the pulse [T] during Phases 1 and 2.

A one-dimensional form of the convection–dispersion equation with two kinetic retention sites was used to simulate nHAP transport and retention in the column experiments (Schijven and Šimůnek, 2002; Bradford et al., 2003):

$$\frac{\partial \theta C}{\partial t}+\rho_b\frac{\partial(s_1)}{\partial t}+\rho_b\frac{\partial(s_2)}{\partial t}=\frac{\partial}{\partial x}\left(\theta D\frac{\partial C}{\partial x}\right)-\frac{\partial qC}{\partial x} \qquad [2]$$

where θ is the volumetric water content (dimensionless), ρ_b is the bulk density of the porous matrix [M L^{-3}], x is the vertical spatial coordinate [L], q is the Darcy velocity [L T^{-1}], and s_1 [N M^{-1}] and s_2 [N M^{-1}] are the solid-phase concentrations associated with Retention Sites 1 and 2, respectively.

The two kinetic retention sites described mass transfer of nHAP between the aqueous and solid phases. The first kinetic site (Site 1) assumes reversible, time-dependent retention, whereas the second kinetic site (Site 2) assumes irreversible, depth-dependent retention as:

Site 1:

$$\rho_b\frac{\partial(s_1)}{\partial t}=\theta\psi_t k_1 C-\rho_b k_{1d} s_1 \qquad [3]$$

Site 2:

$$\rho_b\frac{\partial(s_2)}{\partial t}=\theta k_2\psi_x C \qquad [4]$$

where k_1 [T^{-1}] and k_2 [T^{-1}] are first-order retention coefficients on Sites 1 and 2, respectively, k_{1d} [T^{-1}] is the first-order detachment coefficient, ψ_t is a dimensionless function to account for time-dependent retention, and ψ_x is a dimensionless function to account for depth-dependent retention. Values of ψ_t (Adamczyk et al., 1994) and ψ_x (Bradford et al., 2003) are given by

$$\psi_t=1-\frac{s_1}{s_{\max 1}} \qquad [5]$$

$$\psi_x=\left(\frac{d_c+x}{d_c}\right)^{-\beta} \qquad [6]$$

where s_{max1} [N M^{-1}] is the maximum solid-phase concentration of nHAP on Site 1, d_c is the median diameter of the sand grains [L], and β (dimensionless) is an empirical factor controlling the shape of the spatial distribution. Bradford et al. (2003) found that a value of 0.432 provides an optimum for experiments in which significant depth dependency occurs and that value was assumed in this study.

Breakthrough curves and RPs were analyzed using the HYDRUS-1D code (Šimůnek et al., 2008), which solves Eq. [2–6]. A nonlinear least square optimization routine based on the Levenberg–Marquardt algorithm (Marquardt, 1963) is incorporated in the HYDRUS-1D code to fit the nHAP transport parameters (k_1, k_{1d}, k_2, and s_{max1}). The outlined transport model is viewed as a simple and flexible approach to describe nHAP BTCs and RPs that are not exponential with depth, with retention near the column inlet dominated by irreversible (Site 2) retention and away from the inlet by reversible (Site 1) retention. In this work, we did not attempt to attribute specific nHAP retention mechanisms to a given retention site without additional experimental evidence.

RESULTS AND DISCUSSION

Electrokinetic Properties of Copper-Bearing Hydroxyapatite Nanoparticles and Sand Grains

The electrokinetic potential (ζ potential) will affect the transport and retention behavior of Cu-bearing nHAP. The ζ

potentials of the Cu-bearing nHAP and the sand grains under the different experimental conditions are presented in Table 1. The results indicate that both the Cu-bearing nHAP and quartz sand were negatively charged when the pH ranged from 6.2 to 9.0. The absolute magnitude of the ζ potentials increased with suspension pH due to dissociation of proton groups on the nHAP and quartz sand (Elimelech et al., 1995). These results are consistent with our previous work (Chu et al., 2011; Wang et al., 2011a,b; Zhou et al., 2011) and the reported values of the zero point of charge for nHAP of 4 to 6 (Bouyer et al., 2000) and for quartz sand of 2 to 3 (Sposito, 2008).

The measured ζ potential of the mixture of uncoated and Fe oxide coated sand grains became less negative as the fraction of the Fe oxide coated grains increased (λ = 0–0.36). Elimelech et al. (2000) found a direct relationship between the overall ζ potential of a heterogeneous mixture (uncoated and Fe oxide coated sand grains) and the fraction of positively charged surface on the grains (λ) as

$$\zeta=\lambda\zeta_{\text{Fe-oxide}}+(1-\lambda)\zeta_{\text{quartz}} \qquad [7]$$

where $\zeta_{\text{Fe-oxide}}$ and ζ_{quartz} are the ζ potentials of the Fe oxide coated and clean sand grains, respectively. A similar linear relationship was observed in this study (Fig. 2). Although small values of λ have a minor effect on the ζ potential of the surface charge of heterogeneous porous media, they can have a large impact on the transport of negatively charged colloids (Johnson et al., 1996). We show below that the presence of such small surface charge heterogeneity also has a significant effect on the facilitated transport behavior of Cu associated with nHAP.

Adsorption Isotherms of Copper(II) on Hydroxyapatite Nanoparticles

The Cu-bearing nHAP suspensions used in this work contained 0.1 mmol L^{-1} of total Cu. The quantity of Cu(II) adsorbed on the nHAP as a function of IS at pH 6.2 was reported in Wang et al. (2011a). In this case, around 62.6% of the total Cu was adsorbed on the nHAP and 0.037 mmol L^{-1} of Cu was dissolved in the bulk suspension. Simulation of the equilibrium speciation of Cu using the MINTEQ software indicated that 0.1 mmol L^{-1} of total Cu was undersaturated with respect to potentially precipitating Cu(II) solids.

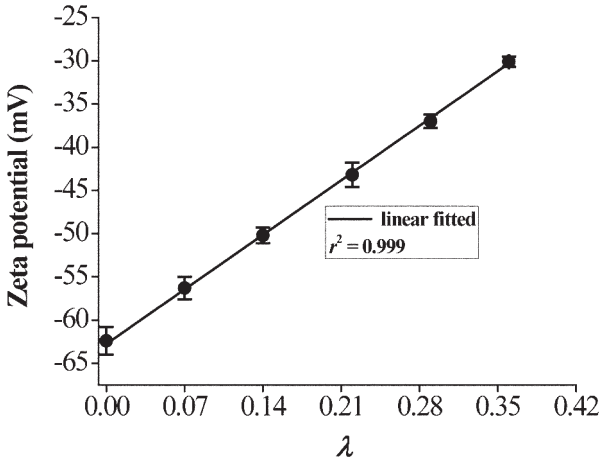

Fig. 2. Overall ζ potentials of the heterogeneous sand grains as a function of the ratio of the mass of Fe oxide coated quartz grains to the total mass of quartz grains (λ) at pH 6.2. Notice that the solid line shows the expected $\zeta = \lambda\zeta_{\text{Fe-oxide}} + (1 - \lambda)\zeta_{\text{quartz}}$ relationship, where $\zeta_{\text{Fe-oxide}}$ and ζ_{quartz} are the ζ potentials of the Fe oxide coated and clean sand grains, respectively. Error bars represent the standard deviations.

The adsorbed quantity of Cu(II) on the nHAP and the concentration of the dissolved Cu(II) under various suspension pH conditions are shown in Fig. 3. The quantity of Cu(II) adsorbed on the nHAP increased from 18.6 to 21.0 g kg^{-1} as the suspension pH increased from 5.0 to 9.0. This is attributed to the increase in negative surface charges of the nHAP with increasing suspension pH (Table 1; Wang et al., 2009). The concentration of the dissolved Cu decreased drastically with increasing suspension pH. This was probably due to the increase in the amount of $Cu(CO_3)_2$ and especially $Cu(OH)_2$ precipitates with increasing suspension pH (Chakoumakos et al., 1979).

Transport and Retention of Hydroxyapatite Nanoparticles and Copper

Effects of Velocity

Figures 4a and 4b present BTCs and RPs, respectively, for nHAP in quartz sand at pore water velocities of 0.22, 0.44, and 2.2 cm min^{-1} and a suspension pH of 6.2. The BTCs are plotted as the fraction of the influent nHAP concentration leaving the packed column, C_i/C_0, as a function of PVs. The RPs are plotted as the normalized concentration (quantity of the Cu-bearing nHAP recovered in the sand, N_t, divided by the quantity in a unit volume of the input nHAP suspension, N_0) per kilogram of dry sand as a function of distance from the column inlet. The corresponding mass recovery of nHAP in the effluent and sand is shown in Table 2. Very good total mass balance was obtained for nHAP (91.6–101%), which provides a high degree of confidence in our experimental procedures.

The nHAP broke through the packed column after 0.9 PV and a plateau was observed after 1.5 PVs for all the tested velocities. The peak effluent concentration of nHAP increased from 0.71 to 0.88 (Fig. 4a) as the fluid pore water velocity increased

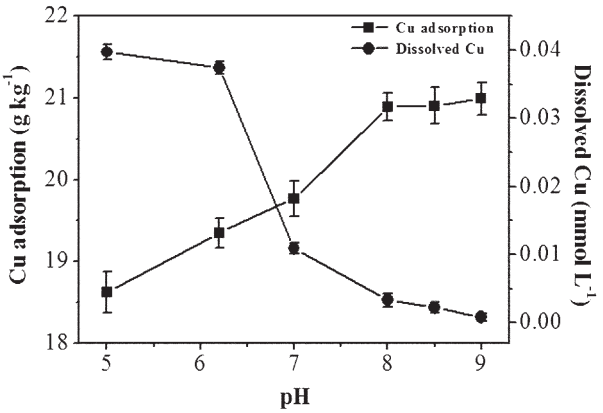

Fig. 3. Adsorbed quantity of Cu(II) on hydroxyapatite nanoparticles and the concentration of dissolved Cu(II) under various suspension pH conditions.

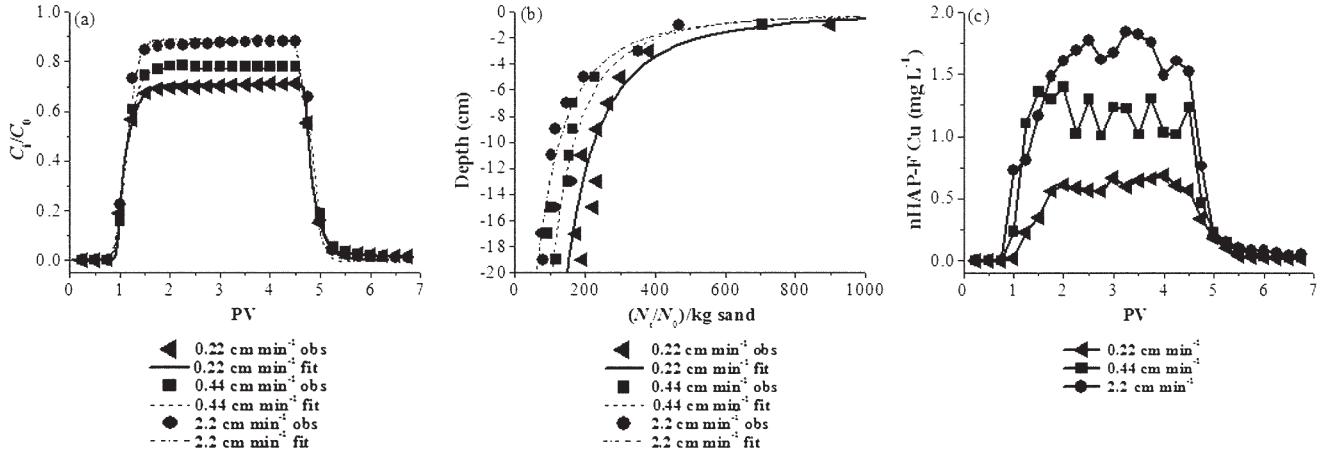

Fig. 4. Measured and fitted (a) breakthrough curves and (b) retention profiles for hydroxyapatite nanoparticles (nHAP) and (c) representative breakthrough curves of hydroxyapatite nanoparticle facilitated (nHAP-F) Cu under the indicated pore water velocity conditions (PV = pore volumes). Fitted curves were obtained using the two-site kinetic attachment model. In (b), the normalized concentrations (quality of the nHAP recovered in the sand, N_t, divided by the quality in a unit volume of the input colloidal suspension, N_0) per kilogram of dry sand are plotted as a function of the distance from the column inlet.

10-fold (from 0.22 to 2.2 cm min^{-1}). The CFT predicts that the attachment rate is proportional to v raised to the 1/3 power (Schijven and Hassanizadeh, 2000). The overall rate of advection, however, is proportional to v such that a systematic decrease in colloid retention is expected with an increase in velocity. The observed nHAP transport shown in Fig. 4a is therefore consistent with this CFT trend. In contrast, Fig. 4b indicates that the RPs for nHAP were not exponential with depth as predicted by CFT. The RPs were actually hyperexponential with depth; that is, greater retention was exhibited in the section adjacent to the column inlet (0–4 cm), with rapidly decreasing retention with depth. The percentage of nHAP retained near the inlet increased from 38.7 to 54.7% as the pore water velocity decreased from 2.2 to 0.22 cm min^{-1}.

The two-site kinetic retention model provided a good description of both the BTCs and the RPs (see R^2 in Table 3 and Fig. 4). Values of the optimized model parameters (k_1, k_{1d}, and k_2) are summarized in Table 3. The value of k_1 slightly increased with increasing pore water velocity, as predicted by CFT. The value of k_{1d} increased with increasing pore water velocity and was actually larger than k_1. This observation suggests that retention on Site 1 is approaching linear equilibrium conditions (van Genuchten et al., 1974). The value of k_2 significantly decreased with increasing pore water velocity. This observation suggests that mechanisms that control nHAP retention near the column inlet are especially sensitive to hydrodynamic forces, as discussed below. Similar behavior has been observed in the literature (Bradford et al., 2007).

Figure 4c shows the BTC for nHAP-F Cu at pore water velocities of 0.22, 0.44, and 2.2 cm min^{-1} and a suspension pH of 6.2. The corresponding mass balance information for the dissolved and nHAP-F Cu in the column effluents is provided in

Table 2. Mass balance percentages (M) of effluent (eff), retained (ret) and total (tot) hydroxyapatite nanoparticles (nHAP) and dissolved (D), nHAP-facilitated (F) and total (tot) effluent Cu (effCu) in the saturated packed column experiments under different pore water velocity (v), pH, and Fe oxide grain coating fraction (λ) conditions.

v	pH	λ	$M_{eff\text{-}nHAP}$	$M_{ret\text{-}nHAP}$	$M_{tot\text{-}nHAP}$	$M_{effCu\text{-}D}$	$M_{effCu\text{-}F}$	M_{totCu}
cm min^{-1}			%					
0.22	6.2	0	72.5 ± 1.1	19.1 ± 2.1	91.6 ± 3.2	44.3 ± 0.7	12.0 ± 1.3	56.3 ± 2.0
0.44	6.2	0	75.8 ± 0.9	15.9 ± 1.8	91.7 ± 2.7	40.3 ± 1.1	18.8 ± 1.7	59.1 ± 2.8
2.2	6.2	0	90.0 ± 0.5	11.0 ± 2.6	101 ± 3.1	40.0 ± 2.3	26.2 ± 0.8	66.2 ± 3.1
0.44	7.0	0	80.6 ± 0.7	14.7 ± 0.9	95.3 ± 1.6	31.1 ± 1.9	23.1 ± 1.2	54.2 ± 2.1
0.44	8.0	0	83.4 ± 0.9	12.5 ± 0.4	95.9 ± 1.3	28.1 ± 1.5	25.9 ± 0.9	60.8 ± 2.4
0.44	8.5	0	90.1 ± 1.0	9.3 ± 0.7	99.4 ± 1.7	19.9 ± 1.7	32.7 ± 1.3	63.3 ± 3.0
0.44	9.0	0	91.0 ± 0.8	8.7 ± 0.6	99.7 ± 1.4	14.6 ± 0.9	43.4 ± 1.2	57.9 ± 2.1
0.44	6.2	0.07	69.9 ± 0.7	10.6 ± 2.3	80.5 ± 3.0	12.6 ± 0.5	11.9 ± 0.7	25.5 ± 1.2
0.44	6.2	0.14	53.7 ± 2.4	18.6 ± 4.3	72.3 ± 6.7	0.6 ± 0.1	5.4 ± 0.4	6.0 ± 0.5
0.44	6.2	0.22	46.6 ± 3.5	24.3 ± 3.4	70.9 ± 6.9	0.6 ± 0.1	4.1 ± 0.3	4.7 ± 0.4
0.44	6.2	0.29	39.6 ± 2.7	29.8 ± 3.8	69.4 ± 6.5	0.7 ± 0.1	3.6 ± 0.2	4.3 ± 0.3
0.44	6.2	0.36	31.9 ± 2.6	35.2 ± 3.5	67.1 ± 6.1	0.1 ± 0.01	3.5 ± 0.02	3.6 ± 0.03

Table 3. Fitted parameters of the two-site kinetic retention model, including the first-order retention coefficient on Site 1 (k_1), the detachment coefficient on Site 1 (k_{1d}), the first-order retention coefficient on Site 2 (k_2), and the maximum solid-phase concentration of hydroxyapatite nanoparticles on Site 1 normalized by the input nHAP concentration (s_{max1}/C_0), as estimated from the breakthrough data for a saturated packed column under different pore water velocity (v), pH, and Fe oxide grain coating fraction (λ) conditions.

v	pH	λ	k_1	k_{1d}	k_2	s_{max1}/C_0	R^2
cm min^{-1}			min^{-1}			(N_t/N_0) kg^{-1}†	
0.22	6.2	0	1.21×10^{-2}	4.35×10^{-2}	7.82×10^{-2}	NA‡	0.972
0.44	6.2	0	1.38×10^{-2}	5.08×10^{-2}	6.74×10^{-2}	NA	0.991
2.2	6.2	0	1.54×10^{-2}	6.27×10^{-2}	2.95×10^{-2}	NA	0.992
0.44	6.2	0	1.38×10^{-2}	5.08×10^{-2}	6.74×10^{-2}	NA	0.991
0.44	7.0	0	1.17×10^{-2}	4.23×10^{-2}	6.43×10^{-2}	NA	0.992
0.44	8.0	0	8.95×10^{-3}	3.94×10^{-2}	4.60×10^{-2}	NA	0.994
0.44	8.5	0	8.04×10^{-3}	3.09×10^{-2}	3.37×10^{-2}	NA	0.995
0.44	9.0	0	3.59×10^{-3}	2.97×10^{-2}	2.31×10^{-2}	NA	0.996
0.44	6.2	0.07	2.54×10^{-2}	NA	4.74×10^{-2}	6.95×10^{2}	0.987
0.44	6.2	0.14	3.07×10^{-2}	NA	6.00×10^{-2}	1.42×10^{2}	0.993
0.44	6.2	0.22	7.29×10^{-2}	NA	6.00×10^{-2}	2.54×10^{2}	0.984
0.44	6.2	0.29	8.12×10^{-2}	NA	6.00×10^{-2}	2.80×10^{2}	0.995
0.44	6.2	0.36	9.22×10^{-2}	NA	6.00×10^{-2}	3.53×10^{2}	0.974

† Quality of the nHAP recovered in the sand (N_t) divided by the quality in a unit volume of the input colloidal suspension (N_0) per kilogram of dry sand.

‡ NA, not applicable because it was neglected.

Table 2. Increasing the pore water velocity enhanced the peak effluent concentration of nHAP-F Cu; that is, nHAP-F Cu increased from 0.69 to 1.85 mg L^{-1} when the pore water velocity increased from 0.22 to 2.2 cm min^{-1}. Similar results were observed by Walshe et al. (2010). Table 2 indicates, however, that nHAP-F Cu accounted for only 12.0 to 26.2% of the total Cu mass and that the dissolved Cu in the effluent ranged from 40.0 to 44.3%. The remaining Cu mass ($1 - M_{totCu}$ = 43.7–33.8%) was assumed to be absorbed onto the low-surface-area but highly negatively charged quartz sand (Table 1). These observations suggest that Cu was transported more efficiently in the dissolved phase than on nHAP and that Cu sorption occurred on the quartz sand and also desorption from Cu-bearing nHAP.

Effects of pH

Figures 5a and 5b present BTCs and RPs, respectively, for nHAP in quartz sand at a pore water velocity of 0.44 cm min^{-1} when the suspension pH was 6.2, 7.0, 8.0, 8.5, and 9.0. The corresponding mass recovery of nHAP in the effluent and sand is shown in Table 2 and indicates very good total mass balance for nHAP (91.7–99.7%). The input nHAP generally broke through at the same time and C_i/C_0 approached to a plateau soon after 1.5 PVs for all the pH tests. Suspension pH had only a minor effect on the nHAP deposition dynamics; however, small increases in the effluent mass recovery occurred when the suspension pH was increased from 6.2 to 9.0 (75.8–91.0%). These results can be explained by changes in the surface charge. As the suspension pH increased (above the pH_{PZC} of nHAP = 4–6), the surface charge of nHAP and quartz became more negative, the depth of the secondary minimum decreased, and the energy barrier to attachment in the primary minimum increased (Table 1). All of these factors produced less retention with increasing pH. The RPs for nHAP shown in Fig. 5b typically exhibited a hyperexponential shape that became more pronounced at lower suspension pH. For example, about 35.1% of the total nHAP retention occurred near the column inlet (0–4 cm) at a pH of 9.0, whereas the value was as high as 45.9% at a suspension pH of 7.0. Similar results were also observed in our previous work (Chu et al., 2011; Wang et al., 2011b).

The two-site kinetic retention model again provided a good description of both the BTCs and the RPs (see Fig. 5 and optimized values of k_1, k_{1d}, and k_2 in Table 3). Values of k_1, k_{1d}, and k_2 all increased with decreasing pH. These observations indicate that nHAP retention on both Sites 1 and 2 depended on the depth of the secondary minimum or the strength of the adhesive interaction.

Figure 5c shows the BTCs for nHAP-F Cu at suspension pHs of 6.2, 7.0, 8.0, 8.5, and 9.0 and a pore water velocity of 0.44 cm min^{-1}. The corresponding mass balance information for the dissolved and nHAP-F Cu in the column effluents is provided in Table 2. Copper synchronously broke through the packed column at about 0.9 PV in the outflow with nHAP. Increasing the suspension pH enhanced the peak effluent concentration of nHAP-F Cu and consequently increased the risk of transporting nHAP-F Cu to subsurface and groundwater environments. As the suspension pH increased from 6.2 to 9.0, the peak effluent concentration of nHAP-F Cu increased more than twofold (from 1.4 to 3.2 mg L^{-1}). Similar results have been observed by Walshe et al. (2010). The increase in nHAP-F Cu transport with pH occurred as a result of the decrease in nHAP retention that was discussed above.

Table 2 indicates that the amount of dissolved Cu in the column effluent decreased with increasing pH, with dissolved Cu accounting for 40.3, 31.1, 28.1, 19.9, and 14.6% of the total Cu

at pH values of 6.2, 7.0, 8.0, 8.5, and 9.0, respectively. Similarly, Chakoumakos et al. (1979) demonstrated that the amount of soluble Cu dramatically decreased as the bulk solution pH increased (also shown in Fig. 3), and the mobility of Cu was significantly inhibited when the bulk solution pH was >8.6 because the most abundant form of Cu was $Cu(OH)_2$ precipitates. The dissolved Cu actually accounted for a greater percentage of the total Cu in the effluent than nHAP-F Cu at pH values of 6.2 and 7.0, whereas the opposite trend occurred at pH values of 8.0, 8.5, and 9.0. This observation indicates that nHAP tended to inhibit Cu transport at lower pH values and facilitated Cu transport at higher pH values. This is due, in part, to greater nHAP retention at lower pH values but also probably reflects an increase in the number of sorption sites for dissolved Cu or the precipitation of Cu on nHAP as the pH increased. The remaining Cu mass ($1 - M_{totCu}$ = 36.7–45.8%) was assumed to be on the sand, and this amount was similar to that reported for the velocity experiments.

Effects of Iron Oxide Grain Coatings

Figures 6a and 6b present BTCs and RPs, respectively, for nHAP in various mixtures of uncoated and Fe oxide coated quartz sand (λ = 0, 0.07, 0.14, 0.22, 0.29, and 0.36) at a pore water velocity of 0.44 cm min^{-1} and suspension pH of 6.2. The corresponding mass recovery of nHAP in the effluent and sand is shown in Table 2. In contrast to experiments examining the effect of velocity and pH, the total mass balance for nHAP became progressively poorer as λ increased (91.7–67.1%). This reflects the influence of the Fe oxide grains on nHAP retention. The nHAP exhibits a negative surface charge at pH 6.2, whereas the Fe oxide minerals are positively charged below their pH_{PZC} (7.5–9, Parks, 1965). Hence, nHAP will strongly attach to the Fe oxide coated grains at pH 6.2 in a primary minimum that is not easily reversible.

Surface charge heterogeneity had a marked effect on the transport of nHAP shown in Fig. 6a. The nHAP broke through at progressively later times and had lower amounts of nHAP in the effluent as λ increased ($M_{eff\text{-}nHAP}$ = 75.8–31.9%). These observations reflect the larger fraction of the surface area that was favorable (Fe oxide) for nHAP attachment. In particular, the amount of attachment was proportional to the favorable Fe oxide surface area and the amount of time it took for nHAP to cover these regions increased with increasing λ. Once the favorable regions were covered, then the remaining nHAP in solution could start to break through in the column effluent.

Figure 6b shows the RPs for nHAP as a function of λ. The RPs do not reflect the complete mass of nHAP in the sand for larger values of λ because of the strong nHAP retention on the Fe oxide coated sand that was not completely recovered during extraction (Table 2). Nevertheless, the amount of nHAP retention tended to increase with increasing λ (Table 2), as expected from the BTCs (Fig. 6a), and the shape of the hyperexponential RPs was consistent with those conducted under various pore water velocity (Fig. 4) and suspension pH (Fig. 5) conditions. These results indicate that the RPs still provide useful information.

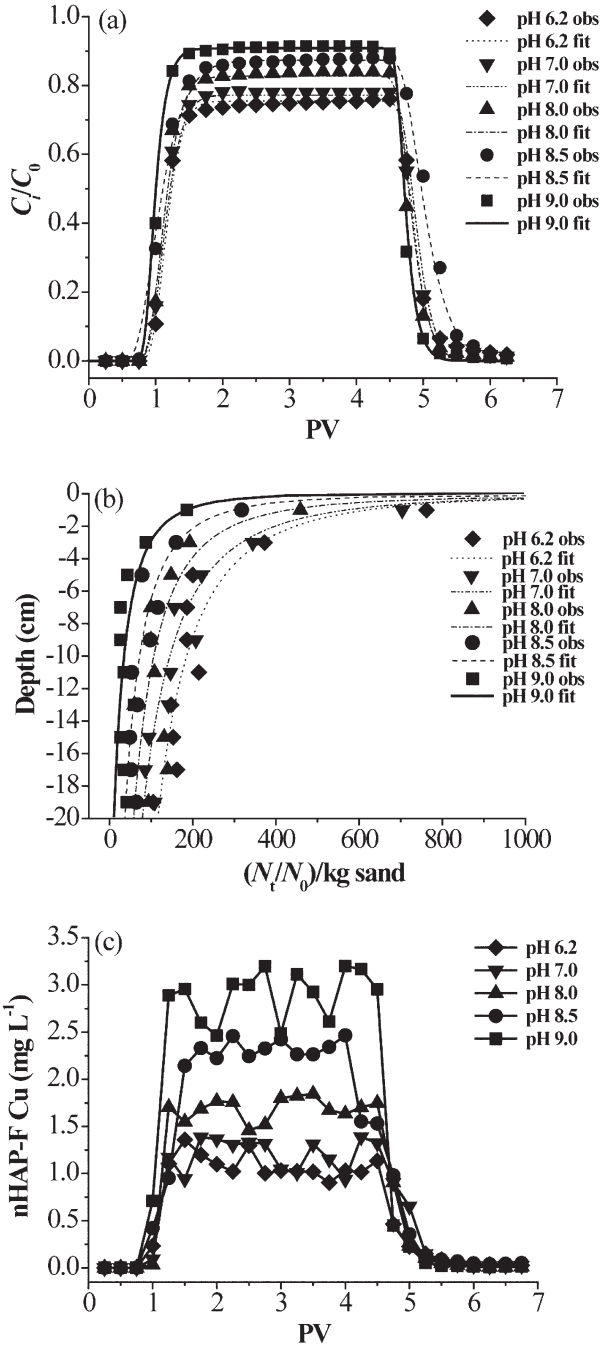

Fig. 5. Measured and (a) fitted breakthrough curves and (b) retention profiles for hydroxyapatite nanoparticles (nHAP) and (c) representative breakthrough curves of hydroxyapatite nanoparticle facilitated (nHAP-F) Cu under the indicated suspension pH conditions (PV = pore volume). Fitted curves were obtained using the two-site kinetic attachment model. In (b), the normalized concentrations (quality of the nHAP recovered in the sand, N_t, divided by the quality in a unit volume of the input colloidal suspension, N_0) per kilogram of dry sand are plotted as a function of the distance from the column inlet.

The retained nHAP concentrations throughout the column increased about 12-fold when λ was increased from 0 to 0.36. This result can be explained by the even distribution of the Fe oxide coated grains (favorable deposition) and nHAP attachment in the packed column.

The two-site kinetic retention model was used to simulate the BTCs for the various uncoated–coated sand mixtures. In

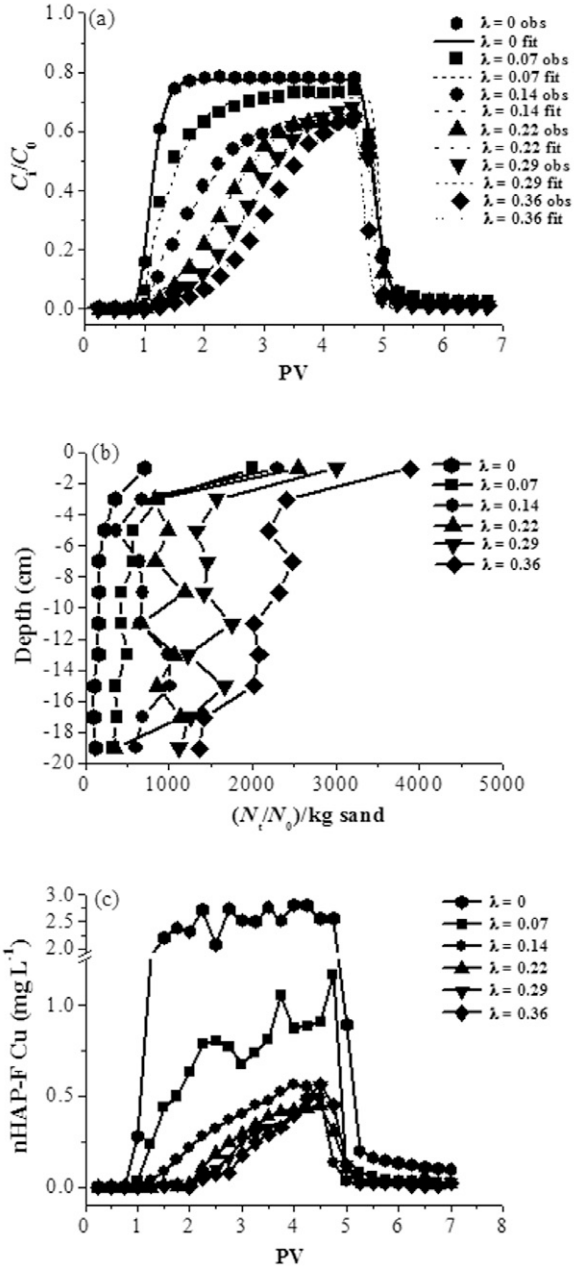

Fig. 6. Measured and fitted (a) breakthrough curves for hydroxyapatite nanoparticles (nHAP), (b) measured retention profiles, and (c) representative breakthrough curves of hydroxyapatite nanoparticle facilitated (nHAP-F) Cu under different Fe oxide coating fraction conditions (λ). Fitted curves were obtained using the two-site kinetic attachment model. In (b), the normalized concentrations (quality of the nHAP recovered in the sand, N_t, divided by the quality in a unit volume of the input colloidal suspension, N_0) per kilogram of dry sand are plotted as a function of the distance from the column inlet.

this case, RPs were not directly used in the parameter optimization because nHAP attachment to the Fe oxide coated sand resulted in mass balance errors (Table 2). The initial values of k_2 in the optimization were selected, however, to be consistent with the observed hyperexponential RP for the λ = 0 system (Fig. 5b). Table 3 provides optimized values of k_1, k_2, and s_{max1}, as well as the R^2. The BTCs were well described using this model (Fig. 6a), and the simulated RPs exhibited similar behavior to the experimental data shown in Fig. 6b. The values of k_2 were relatively insensitive to λ, suggesting that this parameter was mainly controlled by the system hydrodynamics (flow velocity and grain size distribution) at the inlet, as suggested by Fig. 4b. In contrast, values of k_1 tended to increase with λ, which suggests that k_1 was predominantly controlled by the degree of surface charge heterogeneity. A similar result was observed by Chen et al. (2001). Meanwhile, s_{max1} tended to increase with λ. In particular, s_{max1} almost exhibited a one to one correspondence with λ. This trend was expected because s_{max1} is proportional to the fraction of the surface area that is favorable for retention (Chen et al., 2001; Kim et al., 2009; Bradford et al., 2009a). The colloid sticking efficiency, which is proportional to k_1, has been reported to increase in a linear fashion with the patchwise surface charge heterogeneity (Johnson et al., 1996; Elimelech et al., 2000). In contrast, the dependency of k_1 on λ was not as clear in this work, presumably because of the confounding influence of k_2 and s_{max1}.

Figure 6c presents BTCs for nHAP-F Cu in the various mixtures of uncoated and Fe oxide coated quartz sand (λ = 0, 0.07, 0.14, 0.22, 0.29, and 0.36) at a pore water velocity of 0.44 cm min^{-1} and a suspension pH of 6.2. The corresponding mass recovery of dissolved and nHAP-F Cu in the effluent is shown in Table 2. Surface charge heterogeneity had a marked effect on the transport of nHAP-F Cu. The breakthrough of nHAP-F Cu tended to coincide with that of nHAP and exhibited similar retarded and lower effluent concentrations with increasing λ because of nHAP retention. For example, 18.8% of the total Cu was present in the colloidal-associated phase (nHAP-F Cu) at λ = 0 but only 3.5% when λ = 0.36 (Table 2). Dissolved Cu drastically decreased from 40.3 to 0.1% as λ varied from 0 to 0.36 (Table 2). This observation implies that the Fe oxide coated sand had a higher sorption capacity for dissolved Cu than did silica. One potential explanation is the strongly and irreversibly specific adsorption of Cu onto Fe oxide, as observed by Weng et al. (2008).

Mechanisms of Hydroxyapatite Nanoparticle Retention

Factors that influence the retention of nHAP will also have a large impact on the facilitated transport of Cu. Wang et al. (2011b) investigated mechanisms of nHAP retention as a function of NaCl and $CaCl_2$ concentration in the same sand considered in this work. In summary, they found that straining, zones of relative flow stagnation, and the secondary minimum played minor roles in nHAP retention, whereas nHAP surface charge heterogeneity, nHAP aggregation, and surface roughness were more significant factors in nHAP retention. The influence of these same factors is further investigated below under conditions representative of the velocity, pH, and Fe oxide experiments.

Calculated ratios of the size of the nHAP to the sand grain indicate that straining is likely to have been insignificant (Wang et al., 2011b). A shallow secondary minimum occurred in the various velocity and pH experiments, increasing from −0.774 to −0.710 KT (K is the Boltzmann constant, T is the absolute temperature) as the pH increased from 6.2 to 9.0 (Table 1). Increasing amounts

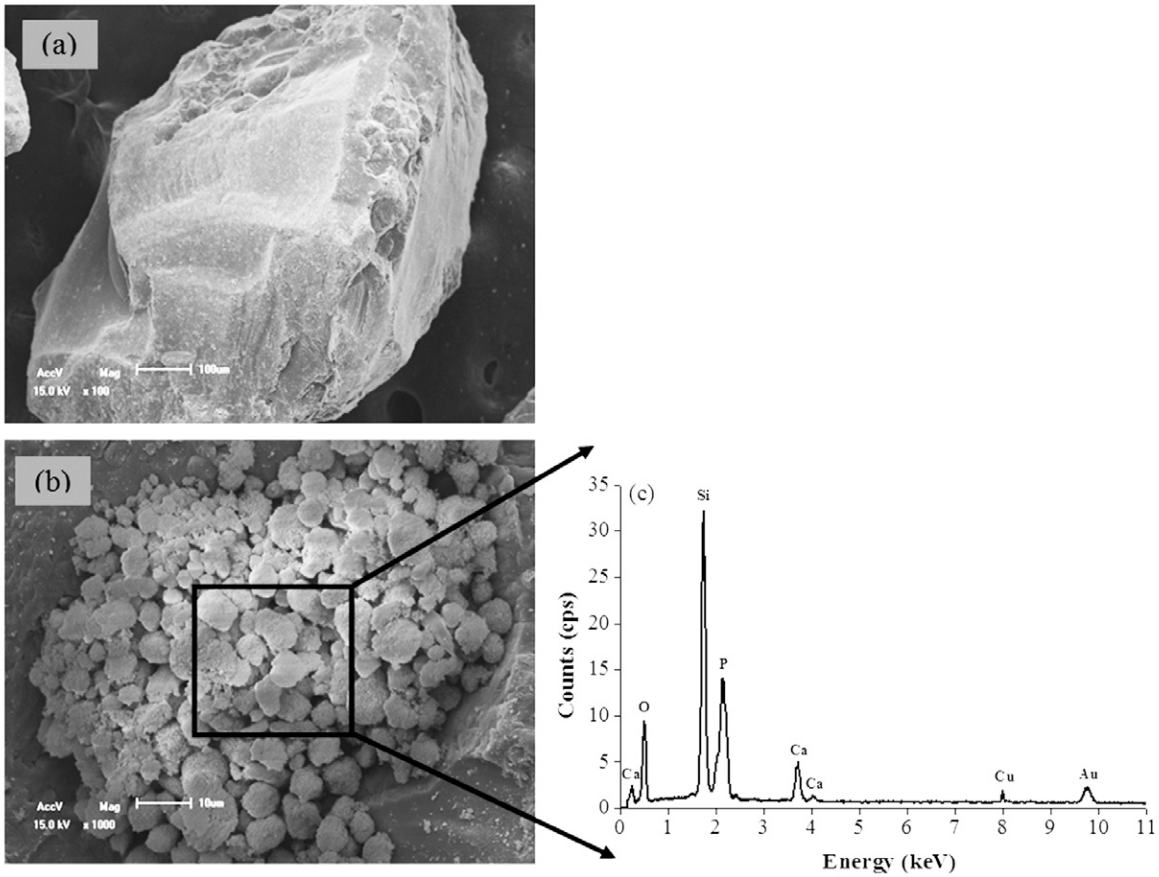

Fig. 7. Scanning electron micrographs of (a) cleaned quartz sand, (b) the quartz sand excavated from the inlet of the packed column after completion of the Cu-bearing hydroxyapatite nanoparticles (nHAP) transport test at suspension pH 7.0, and (c) the corresponding energy dispersive x-ray spectrum of the retained nHAP on the quartz sand in the box.

of nHAP retention occurred with decreasing pH (Fig. 5a), which indicates that the secondary minimum played a role in the retention. A negligible amount of nHAP (0.5%) was recovered during Phase 3, however, when the secondary minimum was eliminated by flushing with ultrapure water (IS = 0) at a suspension pH of 7.0 or following a flow interruption at the end of this experiment (data not shown). These observations confirm the findings of Wang et al. (2011b) that straining, the secondary minimum, and zones of relative flow stagnation played only relatively minor roles in nHAP retention in the pH and velocity experiments.

Surface roughness has been demonstrated to play an important role in colloid retention under unfavorable conditions (Vaidyanathan and Tien, 1988; Yoon et al., 2006; Choi et al., 2007; Torkzaban et al., 2010; Wang et al., 2011b). Figure 7a shows a scanning electron micrograph of a quartz sand grain. The grain possesses surface roughness of different sizes, ranging from several nanometers to dozens of micrometers. Another scanning electron micrograph of the quartz sand excavated from the column inlet after completion of the facilitated transport test at a suspension pH of 7.0 and pore water velocity of 0.44 cm min^{-1} is shown in Fig. 7b. Large, spherical-like aggregates were retained at surface roughness locations in this micrograph. The EDX chemical analysis shown in Fig. 7c indicates that these aggregates were composed of Cu-bearing nHAP. Our previous work also demonstrated that aggregation of nHAP occurred at pH 7.5 and that the aggregation rate increased with decreasing pH (Chu et al., 2011).

The above information indicates that surface roughness and aggregation played important roles in the retention of nHAP in the experiments conducted at different velocities and suspension pH values. In addition to these mechanisms, significant amounts of nHAP attachment occurred in the mixtures of uncoated and Fe oxide coated sand as a result of favorable electrostatic conditions between the negatively charged nHAP and the positively charge Fe oxide surfaces at a suspension pH of 6.2, as discussed above (Table 1).

Hyperexponential RPs occurred during all of the considered experimental conditions of suspension pH and fractions of Fe oxide coated sands but tended to become more exponential in shape at a higher velocity. This observation suggests that hyperexponential profiles are a general phenomenon associated with unfavorable attachment conditions (Table 1) and not necessarily associated with a single retention mechanism.

Surface charge heterogeneity in the colloid population has been reported to cause hyperexponential RPs because the attachment rate increases with increasing (less negative) ζ potentials (Li et al., 2004; Tufenkji and Elimelech, 2005). Wang et al. (2011b) tested this hypothesis by measuring the ζ potential of a nHAP suspension (IS = 0 and pH = 5.7) before and after filtering them through a 1-μm pore diameter glass fiber. The value

of the nHAP ζ potential increased from −53.0 to −60.4 mV after filtering. A similar experiment was conducted in this work at IS = 0.1 mmol L^{-1} and pH 6.2, and the measured nHAP ζ potential increased from −39.5 to −44.7 mV. These observations indicate that some surface charge heterogeneity occurred in the nHAP suspension and this probably contributed to the observed hyperexponential RPs.

The results from the velocity experiments (Fig. 4b) indicate that the amount of nHAP retention near the column inlet was sensitive to hydrodynamic forces. The surface charge heterogeneity hypothesis cannot account for this observation. Bradford et al. (2009b, 2011) demonstrated, using a dual-permeability model, that the shape of the RP was sensitive to the rate of mass transfer to low-velocity regions that are associated with enhanced retention (such as surface roughness, grain–grain contacts, and chemical heterogeneity). Greater amounts of retention occurred at the column inlet because of the advective flux to low-velocity regions, whereas mass transfer to grain surfaces away from the inlet was controlled by sediment, interception, and diffusion as quantified by CFT (Yao et al., 1971). The retention of nHAP at the inlet probably decreased with increasing velocity, probably due to greater hydrodynamic forces that increased the fraction of the surface that was unfavorable for retention (Torkzaban et al., 2007, 2008; Bradford et al., 2011). Alternatively, colloid aggregation has also been reported to contribute to hyperexponential RPs (Chen and Elimelech, 2006, 2007; Chatterjee and Gupta, 2009; Chatterjee et al., 2010), and it is possible that nHAP aggregation on the sand surface is a function of the system hydrodynamics. Additional research is needed to fully resolve these issues but is beyond the scope of this work.

CONCLUSIONS

Packed column experiments were conducted to investigate the facilitated transport of Cu with nHAP under different velocity, pH, and Fe oxide grain coating conditions.

When the pore water velocity increased from 0.22 to 2.2 cm min^{-1} at pH 6.2, the transport of nHAP and nHAP-F Cu increased because of the influence of hydrodynamics on nHAP mass transfer and retention. Dissolved Cu was more efficiently transported than nHAP-F Cu, however, because of nHAP retention and limited Cu sorption and precipitation. The nHAP retention decreased when the solution pH increased because the surface charge of the sand and nHAP became more negative. In addition, dissolved Cu transport decreased with increasing pH because of greater Cu sorption and precipitation. Consequently, the transport of nHAP-F Cu became more significant than that of dissolved Cu when the pH was 8.0, 8.5, and 9.0. Scanning electron microscopy images demonstrated that the nHAP retention was strongly influenced by grain surface roughness and nHAP aggregation in the velocity and pH experiments.

Increasing the fraction of the Fe oxide coatings of the sand produced greater nHAP attachment because of electrostatic interactions between the negatively charged nHAP and positively charged Fe oxide surfaces. Dissolved Cu sorption also dramatically increased on Fe oxide surfaces, presumably due to the high surface area of this coating and amphoteric properties of the Fe oxide surfaces. Consequently, the transport of Cu was almost exclusively controlled by nHAP-F Cu in sand containing Fe oxide coatings.

A two-site kinetic retention model that included provisions for time- and depth-dependent retention provided a good description of all the collected data. The RPs were hyperexponential for the considered velocities, pH values, and Fe oxide coating fractions. These observations suggest that hyperexponential profiles occur under a wide variety of unfavorable attachment conditions. The shape of the RPs and the amount of retention at the column inlet, however, were found to be sensitive to the system hydrodynamics. Retarded BTCs occurred in sands with Fe oxide coatings because of time-dependent blocking and filling of favorable attachment locations.

ACKNOWLEDGMENTS

We thank the financial support from the Knowledge Innovative Project of Chinese Academy of Sciences (KZCX2-YW-Q02-02), the National Basic Research and Development Program (2007CB936604), and the Open Fund of the State Key Laboratory of Soil and Sustainable Agriculture (Y052010027). The participation of M. Paradelo in this study was facilitated by the FPU program of the Spanish Ministry of Education.

REFERENCES

Abudalo, R.A., J.N. Ryan, R.W. Harvey, D.W. Metge, and L. Landkamer. 2010. Influence of organic matter on the transport of *Cryptosporidium parvum* oocysts in a ferric oxyhydroxide-coated quartz sand saturated porous medium. Water Res. 44:1104–1113. doi:10.1016/j.watres.2009.09.039

Adamczyk, Z., B. Siwek, M. Zembala, and P. Belouschek. 1994. Kinetics of localized adsorption of colloid particles. Adv. Colloid Interface Sci. 48:151–280. doi:10.1016/0001-8686(94)80008-1

Baygents, J.C., J.R. Glynn, O. Albinger, B.K. Biesemeyer, K.L. Ogden, and R.G. Arnold. 1998. Variation of surface charge density in monoclonal bacterial populations: Implications for transport through porous media. Environ. Sci. Technol. 32:1596–1603. doi:10.1021/es9707116

Bouyer, E., F. Gitzhofer, and M.I. Boulos. 2000. Morphological study of hydroxyapatite nanocrystal suspension. J. Mater. Sci. Mater. Med. 11:523–531. doi:10.1023/A:1008918110156

Bradford, S.A., and H. Kim. 2010. Implications of cation exchange on clay release and colloid-facilitated transport in porous media. J. Environ. Qual. 39:2040–2046. doi:10.2134/jeq2010.0156

Bradford, S.A., H.N. Kim, B.Z. Haznedaroglu, S. Torkzaban, and S.L. Walker. 2009a. Coupled factors influencing concentration-dependent colloid transport and retention in saturated porous media. Environ. Sci. Technol. 43:6996–7002. doi:10.1021/es900840d

Bradford, S.A., J. Šimůnek, M. Bettahar, M.Th. van Genuchten, and S.R. Yates. 2003. Modeling colloid attachment, straining, and exclusion in saturated porous media. Environ. Sci. Technol. 37:2242–2250. doi:10.1021/es025899u

Bradford, S.A., S. Torkzaban, F. Leij, J. Šimůnek, and M.Th. van Genuchten. 2009b. Modeling the coupled effects of pore space geometry and velocity on colloid transport and retention. Water Resour. Res. 45:W02414. doi:10.1029/2008WR007096

Bradford, S.A., S. Torkzaban, and S.L. Walker. 2007. Coupling of physical and chemical mechanisms of colloid straining in saturated porous media. Water Res. 41:3012–3024. doi:10.1016/j.watres.2007.03.030

Bradford, S.A., S. Torkzaban, and A. Wiegmann. 2011. Pore-scale simulations to determine the applied hydrodynamic torque and colloid immobilization. Vadose Zone J. 10:252–261. doi:10.2136/vzj2010.0064

Chakoumakos, C., R.C. Russo, and R.V. Thurston. 1979. Toxicity of copper to cutthroat trout (*Salmo clarki*) under different conditions of alkalinity, pH, and hardness. Environ. Sci. Technol. 13:213–219. doi:10.1021/es60150a013

Chatterjee, J., S. Abdulkareem, and S.K. Gupta. 2010. Estimation of colloidal deposition from heterogeneous populations. Water Res. 44:3365–3374. doi:10.1016/j.watres.2010.03.025

Chatterjee, J., and S.K. Gupta. 2009. An agglomeration-based model for colloid filtration. Environ. Sci. Technol. 43:3694–3699. doi:10.1021/es8029973

Chen, J.Y., C.H. Ko, S. Bhattacharjee, and M. Elimelech. 2001. Role of spatial distribution of porous medium surface charge heterogeneity in colloid transport. Colloid Surf. A 191:3–15. doi:10.1016/S0927-7757(01)00759-2

Chen, K.L., and M. Elimelech. 2006. Aggregation and deposition kinetics of fullerene (C_{60}) nanoparticles. Langmuir 22:10994–11001. doi:10.1021/la062072v

Chen, K.L., and M. Elimelech. 2007. Influence of humic acid on the aggregation kinetics of fullerene (C_{60}) nanoparticles in monovalent and divalent electrolyte solutions. J. Colloid Interface Sci. 309:126–134. doi:10.1016/j.jcis.2007.01.074

Choi, N.C., D.J. Kim, and S.B. Kim. 2007. Quantification of bacterial mass recovery as a function of pore-water velocity and ionic strength. Res. Microbiol. 158:70–78. doi:10.1016/j.resmic.2006.09.007

Chu, L.Y., D.J. Wang, Y.J. Wang, Y.B. Si, and D.M. Zhou. 2011. Transport behavior of hydroxyapatite nanoparticles in saturated packed column: Effects of humic acid, pH, and ionic strength. (In Chinese.) Environ. Sci. 32:2284–2291.

de Jonge, L.W., C. Kjaergaard, and P. Moldrup. 2004. Colloids and colloid-facilitated transport of contaminants in soils: An introduction. Vadose Zone J. 3:321–325.

Derjaguin, B., and L. Landau. 1941. Theory of the stability of strongly charged lyophobic sols and of the adhesion of strongly charged particles in solutions of electrolytes. Acta Physicochim. URSS 14:733–762.

Elimelech, M., J. Gregory, X. Jia, and R.A. Williams. 1995. Particle deposition and aggregation: Measurement, modeling and simulation. Butterworth-Heinemann, Oxford, UK.

Elimelech, M., M. Nagai, C.H. Ko, and J.N. Ryan. 2000. Relative insignificance of mineral grain zeta potential to colloid transport in geochemically heterogeneous porous media. Environ. Sci. Technol. 34:2143–2148. doi:10.1021/es9910309

Grolimund, D., M. Borkovec, K. Barmettler, and H. Sticher. 1996. Colloid-facilitated transport of strongly sorbing contaminants in natural porous media: A laboratory column study. Environ. Sci. Technol. 30:3118–3123. doi:10.1021/es960246x

Johnson, P.R. 1999. A comparison of streaming and microelectrophoresis methods for obtaining the zeta potential of granular porous media surfaces. J. Colloid Interface Sci. 209:264–267. doi:10.1006/jcis.1998.5908

Johnson, P.R., N. Sun, and M. Elimelech. 1996. Colloid transport in geochemically heterogeneous porous media: Modeling and measurements. Environ. Sci. Technol. 30:3284–3293. doi:10.1021/es960053+

Kim, H.N., S.A. Bradford, and S.L. Walker. 2009. *Escherichia coli* O157:H7 transport in saturated porous media: Role of solution chemistry and surface macromolecules. Environ. Sci. Technol. 43:4340–4347. doi:10.1021/es8026055

Kretzschmar, R.M., M. Borkovec, D. Grolimund, and M. Elimelech. 1999. Mobile subsurface colloids and their role in contaminant transport. Adv. Agron. 66:121–193. doi:10.1016/S0065-2113(08)60427-7

Li, X.Q., T.D. Scheibe, and W.P. Johnson. 2004. Apparent decreases in colloid deposition rate coefficients with distance of transport under unfavorable deposition conditions: A general phenomenon. Environ. Sci. Technol. 38:5616–5625. doi:10.1021/es049154v

Ma, Q.Y., S.J. Traina, T.J. Logan, and J.A. Ryan. 1994. Effects of aqueous Al, Cd, Cu, Fe, Ni, and Zn on Pb immobilization by hydroxyapatite. Environ. Sci. Technol. 28:1219–1228. doi:10.1021/es00056a007

Marquardt, D.W. 1963. An algorithm for least-squares estimation of nonlinear parameters. J. Soc. Ind. Appl. Math. 11:431–441. doi:10.1137/0111030

McCarthy, J.F., and J.M. Zachara. 1989. Subsurface transport of contaminants: Mobile colloids in the subsurface environment may alter the transport of contaminants. Environ. Sci. Technol. 23:496–502.

Parks, G.A. 1965. Isoelectric points of solid oxides, solid hydroxides, and aqueous hydroxo complex systems. Chem. Rev. 65:177–198. doi:10.1021/cr60234a002

Petosa, A.R., D.P. Jaisi, I.R. Quevedo, M. Elimelech, and N. Tufenkji. 2010. Aggregation and deposition of engineered nanomaterials in aquatic environments: Role of physicochemical interactions. Environ. Sci. Technol. 44:6532–6549. doi:10.1021/es100598h

Roy, S.B., and D.A. Dzombak. 1997. Chemical factors influencing colloid-facilitated transport of contaminants in porous media. Environ. Sci. Technol. 31:656–664. doi:10.1021/es9600643

Schijven, J.F., and S.M. Hassanizadeh. 2000. Removal of viruses by soil passage: Overview of modeling, processes, and parameters. Crit. Rev. Environ. Sci. Technol. 30:49–127. doi:10.1080/10643380091184174

Schijven, J.F., and J. Šimůnek. 2002. Kinetic modeling of virus transport at the field scale. J. Contam. Hydrol. 55:113–135. doi:10.1016/S0169-7722(01)00188-7

Silliman, S.E., R. Dunlap, M. Fletcher, and M.A. Schneegurt. 2001. Bacterial transport in heterogeneous porous media: Observations from laboratory experiments. Water Resour. Res. 37:2699–2707. doi:10.1029/2001WR000331

Simoni, S.F., H. Harms, T.N.P. Bosma, and A.J.B. Zehnder. 1998. Population heterogeneity affects transport of bacteria through sand columns at low flow rates. Environ. Sci. Technol. 32:2100–2105. doi:10.1021/es970936g

Šimůnek, J., C.M. He, L.P. Pang, and S.A. Bradford. 2006. Colloid-facilitated solute transport in variably saturated porous media: Numerical model and experimental verification. Vadose Zone J. 5:1035–1047. doi:10.2136/vzj2005.0151

Šimůnek, J., M. Sejna, and M.Th. van Genuchten. 2008. The HYDRUS-1D software package for simulating the one-dimensional movement of water, heat, and multiple solutes in variably-saturated media. Version 4. ICGWMC-TPS-70. Int. Ground Water Model. Ctr., Colorado School of Mines, Golden.

Smičiklas, I., S. Dimović, I. Plećaš, and M. Mitrić. 2006. Removal of Co^{2+} from aqueous solutions by hydroxyapatite. Water Res. 40:2267–2274. doi:10.1016/j.watres.2006.04.031

Sposito, G. 2008. The chemistry of soils. Oxford Univ. Press, New York.

Stahl, R.S., and B.R. James. 1991. Zinc sorption by iron-oxide-coated sand as a function of pH. Soil Sci. Soc. Am. J. 55:1287–1290. doi:10.2136/sssaj1991.03615995005500050015x

Toride, N., F.J. Leij, and M.Th. van Genuchten. 1999. The CXTFIT code for estimating transport parameters from laboratory or field tracer experiments. Version 2.1. Res. Rep. 137. U.S. Salinity Lab., Riverside, CA.

Torkzaban, S., S.A. Bradford, and S.L. Walker. 2007. Resolving the coupled effects of hydrodynamics and DLVO forces on colloid attachment in porous media. Langmuir 23:9652–9660. doi:10.1021/la700995e

Torkzaban, S., H.N. Kim, J. Šimůnek, and S.A. Bradford. 2010. Hysteresis of colloid retention and release in saturated porous media during transients in solution chemistry. Environ. Sci. Technol. 44:1662–1669. doi:10.1021/Es903277p

Torkzaban, S., S.S. Tazehkand, S.L. Walker, and S.A. Bradford. 2008. Transport and fate of bacteria in porous media: Coupled effects of chemical conditions and pore space geometry. Water Resour. Res. 44:W04403. doi:10.1029/2007WR006541

Tufenkji, N., and M. Elimelech. 2005. Breakdown of colloid filtration theory: Role of the secondary energy minimum and surface charge heterogeneities. Langmuir 21:841–852. doi:10.1021/la048102g

Tufenkji, N., J.A. Redman, and M. Elimelech. 2003. Interpreting deposition patterns of microbial particles in laboratory-scale column experiments. Environ. Sci. Technol. 37:616–623. doi:10.1021/es025871i

Vaidyanathan, R., and C. Tien. 1988. Hydrosol deposition in granular beds. Chem. Eng. Sci. 43:289–302. doi:10.1016/0009-2509(88)85041-3

van Genuchten, M.T., J.M. Davidson, and P.J. Wierenga. 1974. An evaluation of kinetic and equilibrium equations for the prediction of pesticide movement through porous media. Soil Sci. Soc. Am. J. 38:29–35. doi:10.2136/sssaj1974.03615995003800010016x

Verwey, E.J.M., and J.T.G. Overbeek. 1948. Theory of the stability of lyophobic colloids. Elsevier, Amsterdam.

Walshe, G.E., L.P. Pang, M. Flury, M.E. Close, and M. Flintoft. 2010. Effects of pH, ionic strength, dissolved organic matter, and flow rate on the co-transport of MS2 bacteriophages with kaolinite in gravel aquifer media. Water Res. 44:1255–1269. doi:10.1016/j.watres.2009.11.034

Wang, D.J., L.Y. Chu, M. Paradelo, W.J.G.M. Peijnenburg, Y.J. Wang, and D.M. Zhou. 2011a. Transport behavior of humic acid-modified nano-hydroxyapatite in saturated packed column: Effects of Cu, ionic strength, and ionic composition. J. Colloid Interface Sci. 360:398–407. doi:10.1016/j.jcis.2011.04.064

Wang, D.J., M. Paradelo, S.A. Bradford, W.J.G.M. Peijnenburg, L.Y. Chu, and D.M. Zhou. 2011b. Facilitated transport of Cu with hydroxyapatite nanoparticles in saturated sand: Effects of solution ionic strength and composition. Water Res. 45:5905–5915. doi:10.1016/j.watres.2011.08.041.

Wang, Y.J., J.H. Chen, Y.X. Cui, S.Q. Wang, and D.M. Zhou. 2009. Effect of low-molecular-weight organic acids on Cu(II) adsorption onto hydroxyapatite nanoparticles. J. Hazard. Mater. 162:1135–1140. doi:10.1016/j.jhazmat.2008.06.001

Weng, L.P., W.H. Van Riemsdijk, and T. Hiemstra. 2008. Cu^{2+} and Ca^{2+} adsorption to goethite in the presence of fulvic acids. Geochim. Cosmochim. Acta 72:5857–5870. doi:10.1016/j.gca.2008.09.015

Yao, K.M., M.M. Habibian, and C.R. O'Melia. 1971. Water and waste water filtration: Concepts and applications. Environ. Sci. Technol. 5:1105–1112. doi:10.1021/es60058a005

Yoon, J.S., J.T. Germaine, and P.J. Culligan. 2006. Visualization of particle behavior within a porous medium: Mechanisms for particle filtration and retardation during downward transport. Water Resour. Res. 42:W06417. doi:10.1029/2004WR003660

Zhou, D.M., D.J. Wang, L. Cang, X.Z. Hao, and L.Y. Chu. 2011. Transport and re-entrainment of soil colloids in saturated packed column: Effects of pH and ionic strength. J. Soils Sediments 11:491–503. doi:10.1007/s11368-010-0331-2